Photoluminescence Lifetime as an Indicator of Temperature in Materials

James Erikson

A senior thesis submitted to the faculty of
Brigham Young University
in partial fulfillment of the requirements for the degree of

Bachelor of Science

John Colton, Advisor

Department of Physics and Astronomy

Brigham Young University

ABSTRACT

Photoluminescence Lifetime as an Indicator of Temperature in Materials

James Erikson
Department of Physics and Astronomy, BYU
Bachelor of Science

Temperature is an important parameter in many processes being studied with microfluidic devices. As such, improved temperature sensing methods compatible with the size and sensitivity required for microfluidics need to be found. This work investigates the photoluminescence lifetime of Rhodamine B and CdTe quantum dots for potential use in microfluidic devices. Lifetime values were sampled over a range of known temperatures through time-correlated single photon counting. Spectral measurements were also taken at each temperature. In Rhodamine B, lifetime was obtained through numerical deconvolution, however, results obtained in this way were unreliable due to variability within the sample itself over time. Similar methods proved similarly unreliable for CdTe quantum dots, which also show variability over time, though to a lesser extent. Through the application of machine learning algorithms, temperatures in CdTe quantum dots can be accurately determined with uncertainties ranging from 7.7 K at cryogenic temperatures to 0.1 K near room temperature. This success shows that temperature dependent photoluminescence is a valid option for future applications in microfluidic devices.

Keywords: photoluminescence, microfluidics, quantum dots, CdTe, lifetime, TCSPC

ACKNOWLEDGMENTS

Many thanks to Dr. John Colton for his advisement and direction with regard to research as well as the writing of this thesis. I'd also like to thank Emma McClure and Charles Lewis for their many contributions to the research described herein. Their efforts have been instrumental in making this work a success.

Contents

List of Figures

Chapter 1

Introduction

1.1 Motivation

In recent years, microfluidics has emerged as an efficient and quick method of analysis in many chemical and biological applications. Through these methods it is possible to integrate entire laboratories onto a single laboratory chip [1], drastically increasing productivity. A challenge presented in this type of analysis, however, is the need for specialized sensors. For instance, conventional thermometers cannot be easily integrated into microfluidic chips, and so other temperature sensing methods must be found.

An effective temperature sensor in a microfluidic device must be small, biologically non-invasive, and provide localized measurements with a short response time. Currently used sensors include thermocouples, nano diamonds, liquid crystals, and fluorescent dyes and quantum dots [2]. Each of these sensors have intrinsic uncertainties. The methods used for data analysis can also contribute to error in temperature predictions. Our goal is to assess the feasibility of photoluminescent materials for use in microfluidic temperature sensors. Photoluminescence data taken at known temperatures can be used to calibrate a method for deducing the temperature using data measured at unknown

temperatures.

1.2 Photoluminescence

Stimulated photoluminescence (PL) is an effective tool for characterizing properties of materials. In general, the PL process consists of three steps: initial excitation, non-radiative settling, and photon emission. The description that follows, given in terms of energy bands, is specific to semiconductors. Even so, the basic principles remain the same for any photoluminescent material.

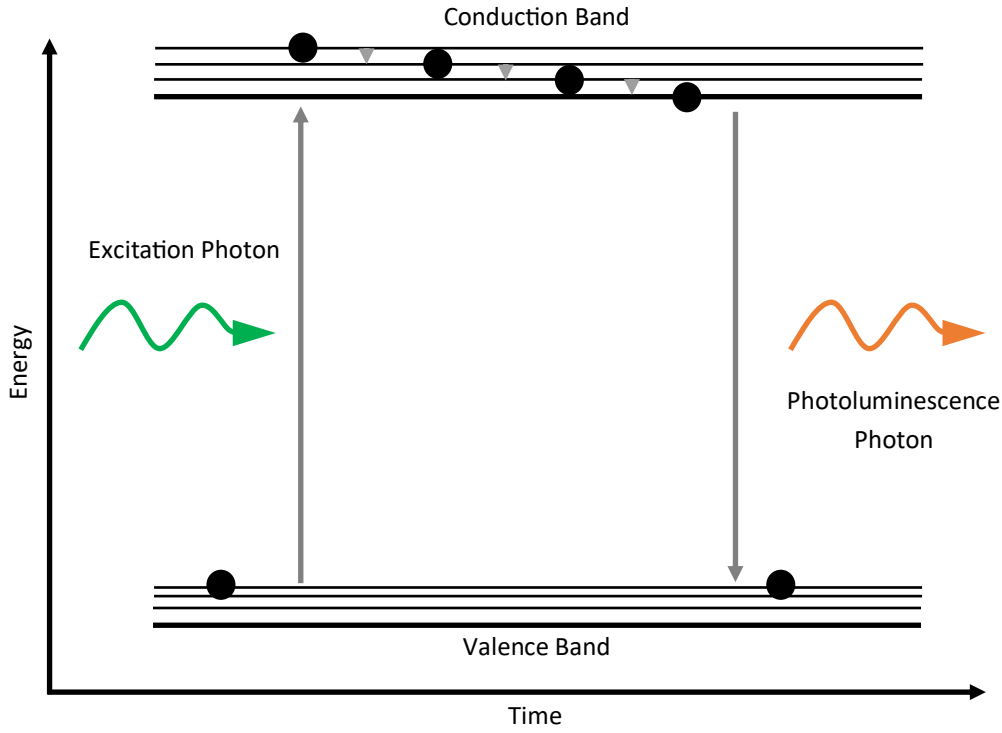

Figure 1.1 The photoluminescence process with time depicted by left-to-right movement. An excitation photon of a higher energy than the band gap causes electrons in the valence band to jump up into the conduction band. Once in this higher energy state, the electron loses energy through non-radiative processes until it is at the lowest unoccupied energy state. It then returns to its initial energy state by releasing a photon with energy equal to the band gap.

To begin the process, electrons within the material's valence band are excited into higher energy states, typically through incursion of a high energy photon. Once in this higher energy state, the electron decays through non-radiative processes within the conduction band to the lowest energy within that band. Finally, with no other ways of reducing its overall energy, the electron jumps back into the highest energy state in the valence band, releasing a photon in the process, as shown in Fig. 1.1. In molecules, the lowest energy of the conduction band is analogous to the lowest unoccupied molecular orbital, while the highest valence band energy is analogous to the highest occupied molecular orbital. Since each emitted photon comes from the same transition, the energy of the PL photons does not vary much, with the energy being material specific. Because of this, PL can be easily measured using a spectrometer to select for the corresponding wavelength.

Multiple parameters can be studied when using PL for analysis. The peak wavelength and intensity of the wavelength spectrum is commonly used to identify defects within crystal structures, as well as assess doping quality and band gap in semiconductors [3]. The time between excitation and photon emission, called the PL lifetime, can also provide valuable information about a material. In particular, within the PL spectrum both the peak wavelength and overall intensity vary with temperature. Similarly, the PL lifetime also shows measurable differences across different temperatures.

While both PL intensity and lifetime exhibit temperature dependence, a lifetime-based model should provide superior predictions. This distinction lies in the overall variability of PL intensity with regard to experimental setup. Since intensity is looking simply at the total number of photons measured, small variations in background light, the excitation source, optical alignment, and even the sample itself can cause the measurements to vary wildly. Such variations can make it nearly impossible to use an intensity-based sensor outside of the lab where it is initially built, and even then it would only be useable with incredible care taken to keep all parameters exactly as they were during calibration. PL lifetime, however, is able to bypass these difficulties as it is purely dependent

on the material itself. A lifetime-based sensor, once calibrated, will be able to function in any lab outfitted to make the measurement, regardless of background noise or other variables. Because of this, this work is primarily focused on PL lifetime measurements, though spectrum measurements are made as well, and form part of our final sensor model.

1.3 Materials

For a material to be considered for use in microfluidic temperature sensors, it must exhibit a certain set of properties. The material must have a high quantum yield, which is the ratio of PL photons emitted vs. the number of excitation photons absorbed. When this ratio is too low, it becomes very difficult to get meaningful PL measurements, and parameters such as the lifetime can be artificially shortened. Likewise, a material must have a fairly well defined PL peak to be analyzed. When a material fluoresces in wide wavelength bands it can be difficult to separate out actual PL from ambient light or noise. Finally, and perhaps obviously, the PL of the material must vary with

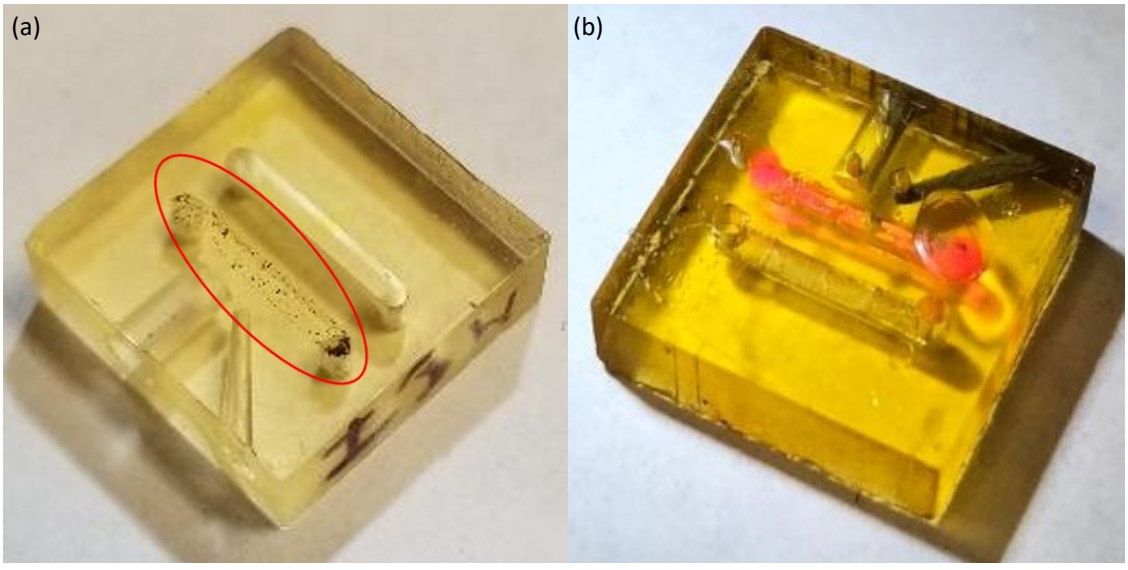

Figure 1.2 Images of resin chips containing samples of (a) CdTe quantum dots and (b) Rhodamine B.

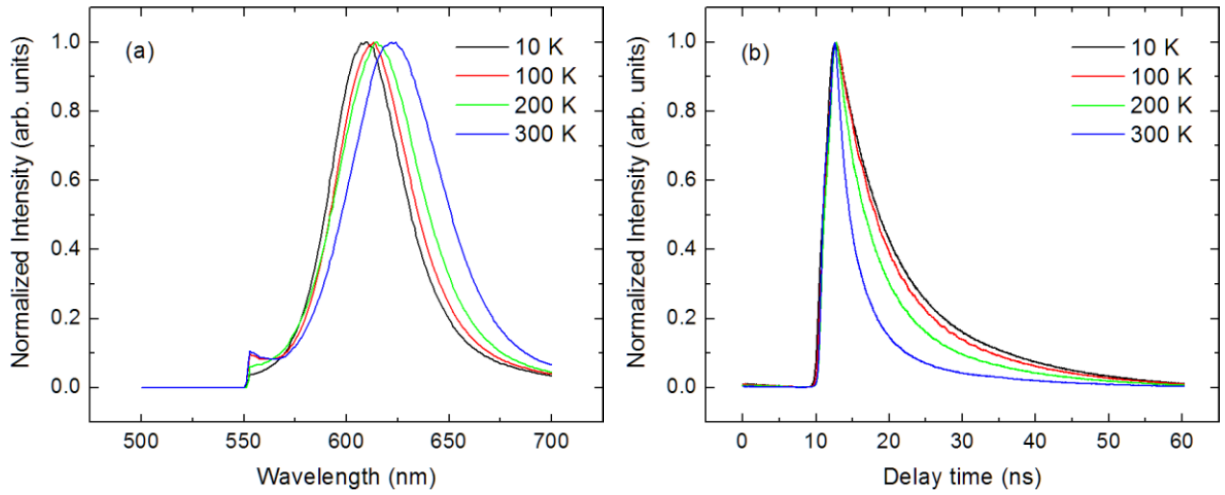

Figure 1.3 Representative plots showing the change in measured PL data from 10 K to 300 K in CdTe quantum dots. Values have been normalized to clearly show shifts. (a) PL spectrum, showing the wavelengths being emitted. (b) Time-resolved PL, showing the rate of decay from higher energy states. The laser pulse arrives after a 10 ns delay, ensuring the full excitation is visible.

temperature. Large changes in the PL as the temperature varies allow a sensor to be more sensitive. Too small of changes limits the potential accuracy and makes the sensor difficult to use. Beyond this, as mentioned in Sec. 1.1, the material samples used must be small, biologically non-invasive, and provide localized measurements with a short response time.

This study focuses on two different materials: Rhodamine B (RB) and CdTe quantum dots (QDs). Rhodamine B is a chemical dye commonly used in biotechnology applications [4]. It is often used as a tracer to track the movements of specific chemicals throughout tissues. Quantum dots are nanoscale semiconductor particles whose properties are dominated by quantum interactions. As such, they have well defined electronic energy bands with separations determined by the size of the particles. The QDs used in this study were sized to emit at 620 nm. Images of the samples used are given in Fig. 1.2. Both of these materials fit the parameters outlined above, they exhibit a high quantum yield and have well defined PL peaks in the wavelength spectrum. The variance of PL with respect to temperature for CdTe QDs can be seen in Fig. 1.3. As temperature rises the peak

wavelength tends to shift towards longer wavelengths, shown in Fig. 1.3(a), while the electrons tend to spend less time in excited states, shown in Fig. 1.3(b). The width of the PL peak of CdTe QDs shown in Fig. 1.3(a) is indicative of a size distribution of the QDs. A sharp shoulder observed near 550 nm is a result of a long-pass filter used to remove stray laser light from the spectrum. The relative shift in peak wavelength is very small, moving approximately 10 nm over a temperature change of 290 K. In contrast, the change in lifetime is much more noticeable. Though not shown, the PL of RB responds in similar fashion.

1.4 Overview

This thesis is split into 5 chapters. Chapter 2 contains an overview of general methods applied to both materials, including experimental setup, data collection methods, and processes for fixing sample temperatures. Chapters 3 and 4 each discuss material specific methods of data analysis and results for Rhodamine B and CdTe quantum dots, respectively. Chapter 5 will restate the conclusions of chapters 3 and 4 and discuss future work to be done.

Chapter 2

General Methods

2.1 Time-Correlated Single Photon Counting

Time correlated single photon counting (TCSPC) is the primary method used to measure the PL lifetime of our samples. The basic principle of operation of this technique is a high speed timing mechanism that is used to record the time between two external triggers. In this case, a start trigger is supplied using a pulse generator. The stop trigger is sent by a detector once a PL photon has been measured.

A typical TCSPC measurement begins with a reference pulse that triggers the charging of a capacitor within the TCPSC module. The capacitor charges at a known rate, which allows the amount of charge stored in the capacitor to serve as a record of how much time has passed. Once a PL photon is measured the module halts the charging, and the stored charge is measured and converted into a time value. This value is recorded in a histogram, and the process is repeated. After many cycles, the generated histogram becomes an accurate representation of the time-resolved PL from which the lifetime can be extracted.

While the theory behind TCSPC is fairly simple, a number of practical complications must be

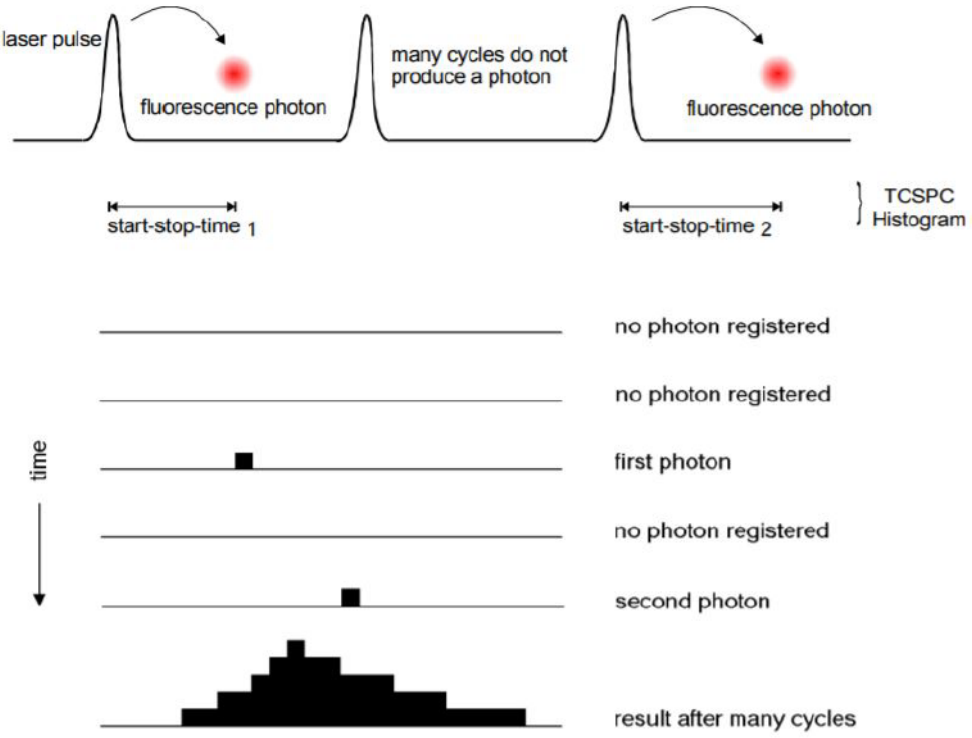

Figure 2.1 Process of generating a histogram with TCSPC. A maximum of one photon is measured per pulse and subsequently added to the histogram. From Ref. [5]

accounted for. The first are dead time and data pile-up. As seen in Fig. 2.1, measurement time can be divided into bins marked on each end by laser pulses. Whenever a photon is measured, the capacitor used for timing must be discharged before another can be recorded. This timing limitation, combined with the mechanism's reliance on reference pulses to provide start triggers, results in a practical maximum of a single photon measured per bin. As a result, a bin containing more than one photon only records the first, and any others are lost. If this occurs in a large number of bins, the resulting histogram is skewed towards shorter times, resulting in an inaccurate representation of the lifetime of the sample. To remedy this, incoming PL is attenuated through the use of neutral density filters so that the PL photon count is less than five percent of the reference pulse frequency. The lower count rate ensures that on average a photon will be measured in one out of every 20 bins. Using a Poisson distribution, a count rate of five percent of the reference pulse frequency

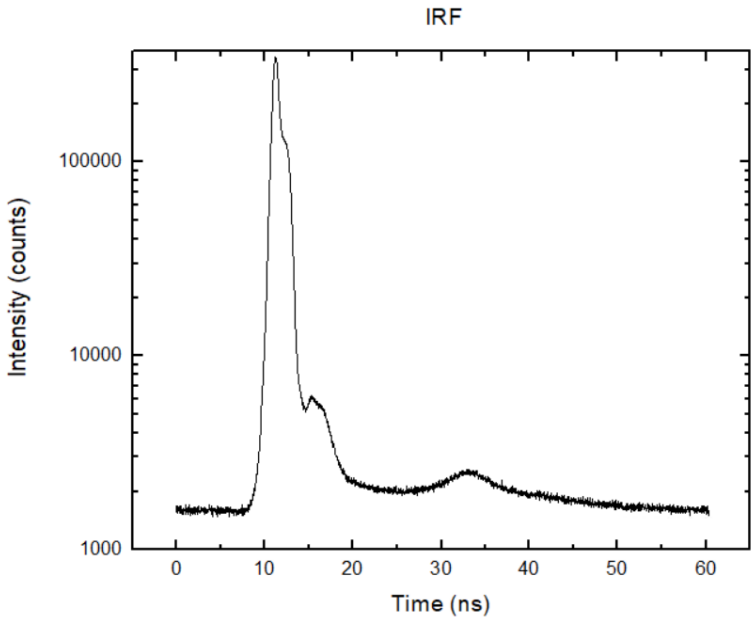

Figure 2.2 Measured IRF histogram taken with the same setup as normal TCSPC data collection, the only difference being the replacement of the sample with a scattering agent (colloidal silica). The laser pulse width and irregularities in pulse shape are clearly seen. This IRF also includes smaller contributions from other factors, such as detector response time and spectrometer slit size.

corresponds to a 0.119 percent probability[1] of two photons being measured in the same bin. This provides ample time for the timing mechanism to reset while also avoiding photon pile-up [6].

A final consideration to be accounted for is the equipment response. All measurements are taken with non-ideal equipment, and as a result the histogram produced by TCSPC includes artifacts from those extra contributions. Primary issues that must be accounted for include the width of the laser pulse, irregularities in the laser pulse, spectrometer slit size, and non-zero response time of the detector itself. The combination of these issues is known as the instrument response function (IRF). To extract the PL lifetime from TCSPC data, the IRF must be removed from the measured data through a deconvolution process. A representative plot of the IRF measured for our setup is given

[1] The probability of k events occurring in an interval is given by $P(k) = \frac{\lambda^k e^{-\lambda}}{k!}$ where λ is the event rate. Using $\lambda = 0.05$ and $k = 2$ gives a result of 0.00119, or 0.119 percent probability of two photons arriving in one bin.

in Fig. 2.2.

The basic setup used for PL measurements is shown in Fig. 2.3. The configuration shown is specific to time correlated single photon counting (TCSPC) measurements, but spectral PL data is also taken using a similar setup. A 520 nm laser (Thorlabs TCLDM9 diode laser) is used to excite the PL. The laser is pulsed using a pulse generator (Agilent 81110A) through a bias-T connection. The pulse generator is set to give 5 ns laser pulses every 60 ns with an average power of 0.2 mW. After the sample is excited, the PL is collected with a lens, which collimates the emitted light and sends it through a 550 nm long pass filter to remove scattered laser light. The PL is then focused into a spectrometer (JY Horiba Triax 550) which selects for the wavelength of interest (approx. 620 nm for CdTe QDs). The PL is then measured by a photomultiplier tube (PMT). For time resolved PL measurement the pulse generator also sends a signal to trigger the TCSPC module. Once the PMT measures a photon, another signal is sent to the module to trigger the stop. The time between the two trigger signals is then measured and recorded as a data point for time resolved PL.

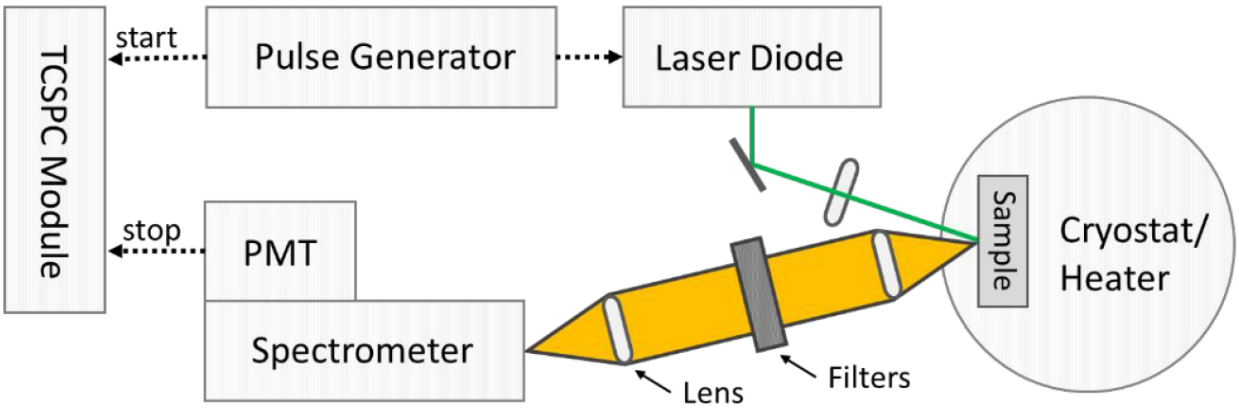

Figure 2.3 Optical experiment setup. Pulse generator sends out two signals, one to the TCSPC module to start a timer, the other to a 520 nm laser diode. The resulting laser pulse excites photoluminescence (PL) in the sample, which is held at a known temperature in a cryostat or heater. Emitted light is then collected and focused into a spectrometer. PL is then measured using a photomultiplier tube (PMT), which sends a signal to the TCSPC module to stop the timer.

2.2 Photoluminescence Spectra

While not directly useful for determining the PL lifetime of a material, measurement of the wavelength spectrum provides valuable information for correlating optical properties with temperature. The process is similar to that described in Fig. 2.3 with the omission of the TCSPC module. A spectrometer is used to sweep a range of wavelengths and observe the resulting signal on the detector. This information identifies the peak wavelength used in TCSPC as well as gives an idea of the quality of the sample. In quantum dots, for example, a wider principle peak indicates a larger distribution of dot size. Presence of peaks other than those expected from the sample are often indicators of contaminants or other defects. Since these defects can affect the PL lifetime, it is important to observe the PL spectrum of a sample to confirm the accuracy of lifetime measurements.

Because the spectrum also has some temperature dependence, it can be used alongside the lifetime data to correlate with temperature. In CdTe quantum dots for example, a redshift was observed in the spectral peak as temperature increases (see Fig. 1.3). This dependence was ultimately used in a model designed to predict temperature in CdTe. This is addressed in more detail in Chapter 4 of this thesis.

2.3 Temperature Control

To correlate PL with temperature, spectra and lifetimes were measured over a wide range of known temperatures. Temperature was split into two regimes: low temperature, ranging from 10K to 300K; and high temperature, from 298K to 319K. The split was done to better assess the utility of a PL based temperature sensor. The low-temperature regime provides a view of sensor response over a wide range. The high-temperature regime is a more accurate representation of the range where such a sensor would actually be used. As such, higher accuracy in the high-temperature range is desired.

The low-temperature regime was done using a commercially made cryostat (Cryo Industries

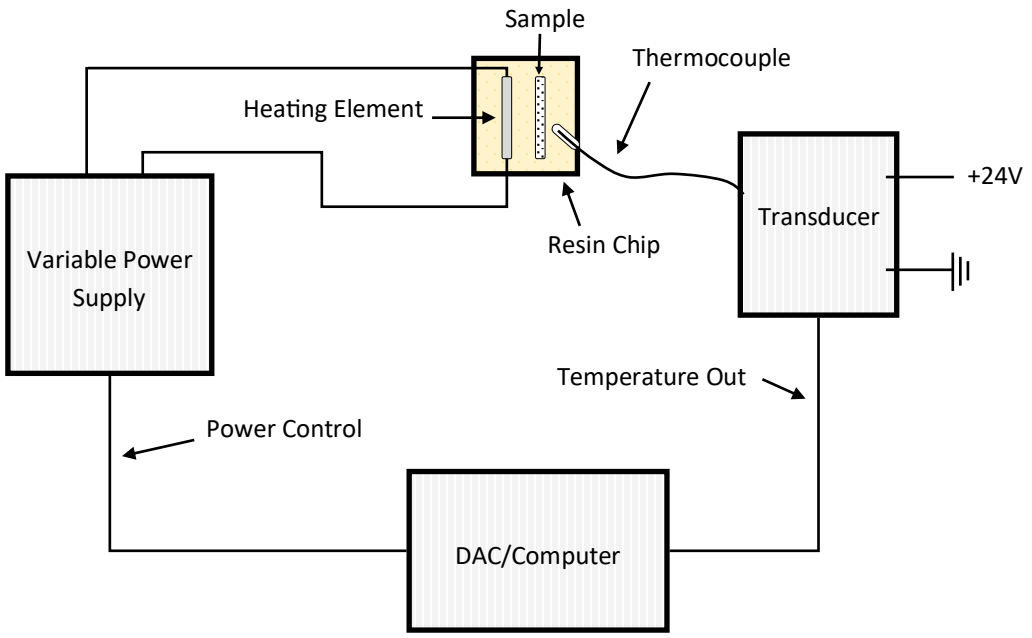

Figure 2.4 Heating stage setup. Current temperature is measured using a thermocouple. Temperature output is recorded using a thermocouple-measuring transducer and sent on to a computer via a DAC board. A LabVIEW VI then employs a PID controller to determine necessary output power. This power is sent on to a variable power supply, which applies a current to a heating element embedded in the same chip that houses the sample. The new temperature is measured by the thermocouple, and the cycle is repeated, forming a feedback loop. This process allows the temperature to stabilize at the desired value.

custom-designed closed cycle cryostat) with built in temperature control. PL data was recorded in steps of 10 K throughout the low range for CdTe QDs and in steps of 30 K for RB.

The high-temperature regime is achieved using a home-built temperature controller employing a PID feedback loop. The resin chip that holds the sample was outfitted with three channels: one for the sample itself, one for a heating element, and a third designed to get a thermocouple as close to the sample as possible (see Fig. 2.4). Galinstan, a gallium based liquid metal, is chosen as the heating element. This metal has a low viscosity, which allows it to fill the channel, and a high enough resistivity to provide heat when a current is run through it. As the thermocouple (TC, Type K, OMEGA Engineering) measures the current temperature, the signal is sent through a thermocouple-measuring transducer (Phoenix Contact MINI MCR-SL-TC-UI-2864448) to a

computer through a DAC board. A LabVIEW VI then determines how much current should be applied to the heating element using a PID controller. This current is supplied by a DC power source (BK Precision 1696) controlled by the same VI. As the applied current heats the sample, the temperature is again measured by the thermocouple and the cycle is repeated, completing a feedback loop. This allows the temperature to be controlled to within approximately 0.1 K. In the high temperature regime PL data was recorded in steps of 1 K between 298 K and 319 K for CdTe QDs. High temperature data was not taken for RB. For more details on operation of the heating stage, see Appendix A.

2.4 Numerical Deconvolutions

As described in section 2.1, measured TCSPC data includes artifacts resulting from the width of the laser pulse, irregularities in the laser pulse, spectrometer slit size, and detector response time, together known as the instrument response function (IRF). This added response must be removed from the measured data in order to extract the true decay curve and, by extension, the PL lifetime.

The IRF is removed through a numerical deconvolution process known as iterative reconvolution. Once TCSPC data has been taken, the IRF is recorded by removing the sample and scattering laser light into the detector while an equivalent measurement is done. With the IRF in hand, the standard procedure for analysis is followed as outlined in Ref. [7]. The first step is to assume a functional form for the actual decay. From there, an arbitrary set of initial parameters is selected to create a test function for the decay. This test function is then convolved with the measured IRF and the result compared to the measured TCSPC data. A regression fit is then done on the test function in order to minimize the difference between the convolved result and the measured data. Once the fit is complete, the lifetime value can be determined from the final parameters of the test function.

This success of this method is highly dependent on choosing the correct form of the decay.

In simple cases a single exponential decay may adequately describe the process. When multiple processes are involved in the decay itself, two or more decay mechanisms may need to be accounted for, each with a corresponding amplitude and lifetime. At the extreme end a continuum of decay mechanisms can exist [8].

For both Rhodamine B and CdTe multiple functional forms were assessed. Deconvolutions were then done at each temperature using the best decay function for each material in an attempt to describe the temperature dependence of the PL.

This concludes treatment of methods common to both Rhodamine B and CdTe quantum dots. Chapter 3 includes discussion of specific methods and results for Rhodamine B. Chapter 4 focuses on CdTe quantum dots, including a machine-learning based method for temperature prediction that ultimately superseded the deconvolution method of characterizing TCSPC data.

Chapter 3

Rhodamine B

3.1 Deconvolutions

The numerical deconvolution method described in Sec. 2.4 (iterative reconvolution) was the primary data analysis method used for Rhodamine B. In this case, the test function settled upon was a simple exponential decay:

$$f(t) = A \exp\left(-\frac{t - t_0}{\tau}\right) \tag{3.1}$$

Here the lifetime is represented by the parameter τ, with the two other fitting parameters being the amplitude A, and the left/right shift t_0.

3.2 Results

Lifetime data was collected at 11 temperatures between 15 K and 300 K. The resulting values are plotted in Fig. 3.1. A general downward trend can be observed in the lifetimes as temperature increases, though this only becomes apparent above 180 K. Similar measurements taken at different times or with different samples are also depicted. The three data sets shown range in sample age, with a freshly prepared sample (black), a sample after 3-4 months (red), and a sample after 9+

months (green). The PL of Rhodamine B samples appears to degrade over time, as evidenced by the general decrease in lifetimes as time passes. After extended periods, the trends exhibited by fresher samples also begin to degrade. This is especially evident in lower temperature ranges.

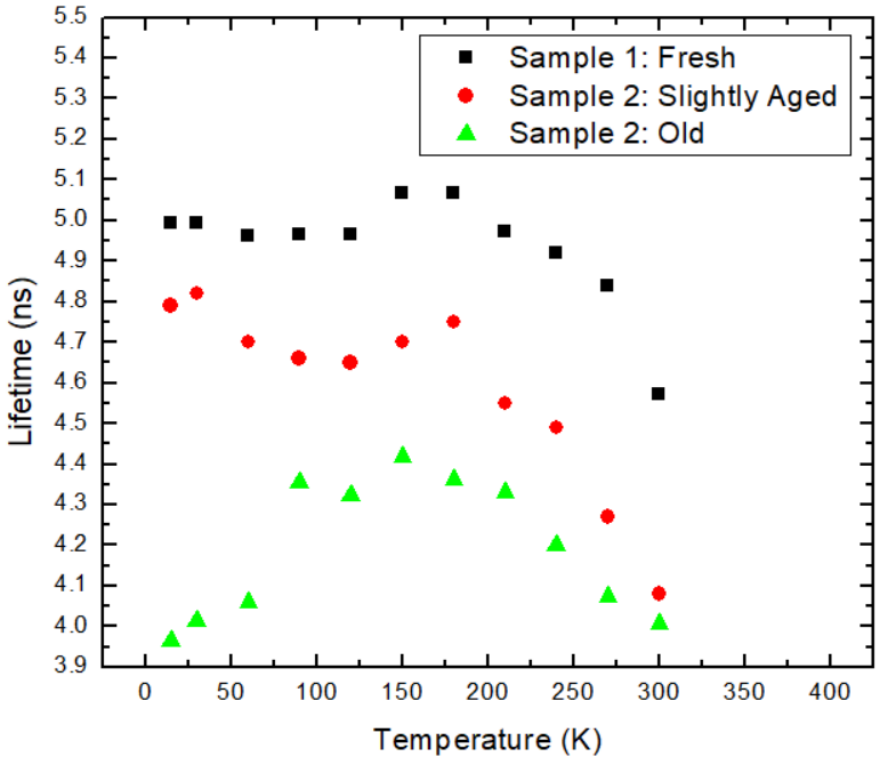

Figure 3.1 Lifetime values of Rhodamine B. Measurements were taken with samples at varying times since their preparation, showing a general decrease in lifetime as the sample ages. No data was taken above 300 K.

3.3 Conclusions

The photoluminescence lifetimes of Rhodamine B do exhibit temperature dependence between 15 K and 300 K. General trends toward shorter lifetimes as temperature increases are present. However, the PL appears to be dependent on the age of the sample as well. Because of this, a temperature sensor incorporating Rhodamine B would need to be recalibrated often to remain accurate. In

addition, the lifetimes only begin to show significant changes above 200 K. This high variability and need for constant recalibration make Rhodamine B an unreliable choice for a temperature sensor. In light of these shortcomings, data was not taken above 300 K with Rhodamine B.

Chapter 4

CdTe Quantum Dots

4.1 Deconvolutions

While Rhodamine B exhibits a simple PL decay, deconvolution fits on CdTe quantum dots (QDs) require a more complex test function. Similarly good fits were obtained using both a double exponential decay (4.1) and a stretched exponential decay (4.2) test function.

$$f(t) = A\exp\left(-\frac{t-t_0}{\tau_1}\right) + B\exp\left(-\frac{t-t_0}{\tau_2}\right) \tag{4.1}$$

$$f(t) = A\exp\left[-\left(\frac{t-t_0}{\tau}\right)^{\beta}\right] \tag{4.2}$$

The results of these fits are given in Fig. 4.1. The large number of fitting parameters and the relative insensitivity of the fits on some of the parameters create a large uncertainty in the fit results. To quantify that uncertainty, each fit was repeated 100 times on the same data set using slightly different starting parameters each time. With more parameters it becomes possible to get low error fits with a wider range of final results. This effect is less pronounced in the stretched exponential fit, though still present. Even with the lower number of parameters, the overlap in uncertainties between different temperatures would make it nearly impossible to determine the temperature from a lifetime measurement.

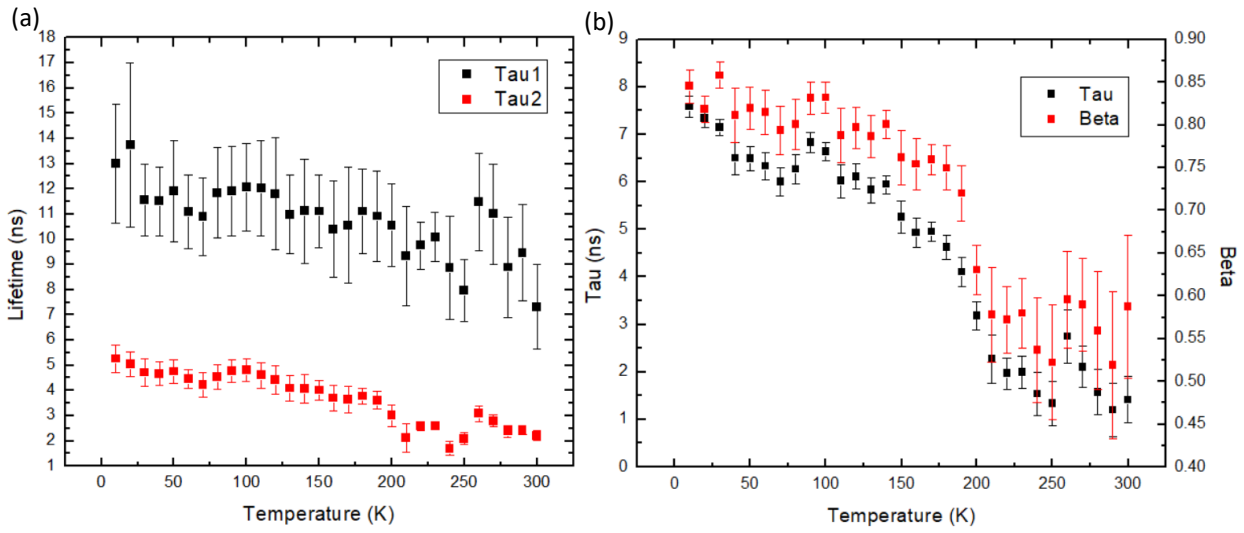

Figure 4.1 Results of deconvolution fits done using a (a) double exponential decay and (b) stretched exponential decay. Fits were done 100 times for each temperature to produce the points and error bars. All τ values have units of ns. β is a unitless quantity.

In light of this shortcoming, a different method of data analysis is necessary. A machine learning architecture could provide higher accuracy while avoiding the uncertainties inherent in the deconvolution method.

4.2 Machine Learning

To avoid the difficulties of deconvolution methods, a neural network was trained using TCSPC and spectral data sets. Before the training could begin, however, the data was preprocessed in two different ways. First, the TCSPC data was run through a logarithm operation. This allowed the exponential nature of the decay to take on a more linear shape, giving more weight to points at later times. Second, a (0,1) min-max normalization was done on both the TCSPC and spectral data. This was done to increase the usability of the network in different situations. Variations in optical alignment and detector sensitivity among other parameters can cause large changes in the intensity of PL measured. A min-max normalization removes this uncertainty, and allows the

resulting network to be useful in different situations.

Two neural networks were trained, one for each of the two temperature regimes as described in Sec. 2.3. The low-temperature regime used data from 30 temperatures (ranging from 10 to 300 K in steps of 10 K). The high-temperature regime used data from 22 temperatures (ranging from 298 to 319 K in steps of 1 K). From these temperatures data was separated into 3 distinct sets for the training process. The first, called the "training set," consists of approximately 80 percent of the original data set. This set was used to train the network. Secondly, the "testing/validation set," which was used to test the neural network throughout the training process. This set contains the majority of the remaining 20 percent of the temperatures. Finally, the "holdout set," is a group of five randomly selected temperatures from each regime that were left out of the entire training process. These temperatures were used after the training was complete to assess the overall accuracy of the network.

In general, effective training of a neural network requires a large amount of data, much more than the 30 or 22 temperatures measured in each regime. To remedy this problem, the data was augmented using a cubic spline interpolation. In the low-temperature regime, interpolation was done in steps of 1 K using the training and testing sets. This resulted in a set of 291 pairs of spectral and TCSPC data ranging between 10 and 300 K. In the high-temperature regime, interpolation was done in steps of 0.1 K, resulting in 211 pairs of spectral and TCSPC data between 298 and 319 K.

Once the data was prepared, the networks were trained using a mean squared error loss function over 6000 training epochs using the training and testing sets. After the training, the performance of the networks was assessed using the holdout set. For a more in-depth treatment of the machine learning process used, see senior thesis by Charles Lewis [9].

4.3 Results

The accuracy of the neural networks is determined using the mean absolute error (MAE) of the holdout set in each regime. The individual networks' predictions and accuracy are depicted in Fig. 4.2. The temperature values predicted by the networks are plotted relative to their true values. As such, the accuracy can be qualitatively determined by how close the points fall to the line $y = x$. In the low-temperature regime, the network is effective except at two temperatures in the holdout set: 70 and 90 K. Using the whole range the MAE of the holdout set for the low-temperature regime is 7.7 K. When restricting the range assessed to only temperatures above 100 K the MAE is 0.4 K. In the high temperature regime, the network is even more accurate, despite the wiggles that can be seen, which are due to the magnified temperature scale. The MAE for this regime is 0.1 K.

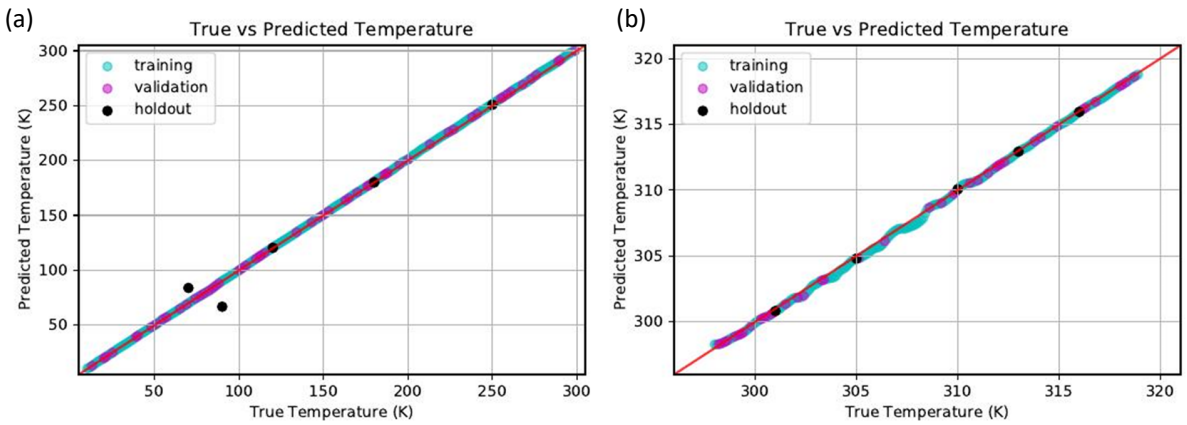

Figure 4.2 Actual vs Predicted temperatures for both temperature regimes. Points lying closer to the line $y = x$ are more accurate. The results for the low-temperature neural network are shown in (a) while the high-temperature regime is shown in (b). Overall, the accuracy was high for both regimes with the exception of the 70 K and 90 K holdout points in the low-temperature regime. Over the whole range in (a) the mean absolute error (MAE) of the holdout set was 7.6 K, however over the range from 100 to 300 K the MAE drops to only 0.4 K. In (b) the MAE was 0.1 K.

4.4 Conclusions

Both the time-resolved photoluminescence and the photoluminescence spectrum of CdTe quantum dots exhibit temperature dependence between 10 K and 319 K. Due to the complex nature of the CdTe PL decay function, standard deconvolution methods could not be used to analyze the time-resolved PL. Instead, neural networks were trained to predict temperature using the full TCSPC and spectral data sets. The networks were highly accurate, especially in the high-temperature regime, which was representative of the temperature range at which a microfluidic temperature sensor might actually be used. CdTe quantum dots were found to be effective as a temperature sensing agent in microfluidic devices.

Chapter 5

Conclusions and Future Work

Rhodamine B and CdTe quantum dots were assessed for use in a photoluminescence-based microfluidic temperature sensor. The temperature dependence of Rhodamine B PL was analyzed using a numerical deconvolution analysis method. Results showed that the PL lifetimes exhibit temperature dependence, though the dependence is only consistent above 200 K. Measurements taken months apart also showed that the PL lifetimes tend to change over time as the sample degrades. The limited range of usefulness and the need for constant recalibration due to sample decay make Rhodamine B an unreliable choice for a temperature sensor. Due to the lack of promise shown by Rhodamine B, no measurements were made above 300 K.

Assessment of CdTe quantum dots proved difficult using deconvolution analysis. The necessary forms of the decay function had too many parameters for the PL lifetime to be accurately determined by the regression methods involved. Instead, machine learning methods were employed to take the raw spectral and TCSPC data and use them to predict the temperature. Two networks were trained, one for each temperature regime. The networks were highly accurate, especially in the high-temperature regime. Given the success of the network over the range representative of where a microfluidic temperature sensor might be used, it was concluded that the PL of CdTe quantum dots is a viable choice for these sensors.

Looking forward, the next step is to test other types of quantum dots. CdTe is effective for temperature sensing, but comes with its own drawbacks. After long periods the photoluminescence of the QDs changes sufficiently that the network must be retrained in order to remain effective. Other materials may not show those same changes in PL while retaining, or even improving upon, the level of accuracy seen in CdTe.

Appendix A

Heating Stage Operation

The home-built temperature controller used for high-temperature regime measurements is described in Sec. 2.3. Once the system has been built in accordance with the schematic given in Fig. 2.4 there are some further operational quirks that should be understood for the heater to operate properly.

Following the same order described in Fig. 2.4, a feedback loop is formed beginning when the temperature is measured by a thermocouple (TC, Type K, OMEGA Engineering) using a thermocouple-measuring transducer (Phoenix Contact MINI MCR-SL-TC-UI-2864448). A computer uses the measured temperature and a set target temperature to determine the current that should be sent on to a heating element embedded in the chip housing the sample. This current is supplied by a DC power supply (BK Precision 1696) controlled by the computer, allowing the sample to be heated or cooled as required.

The thermocouple-measuring transducer used (Phoenix Contact MINI MCR-SL-TC-UI-2864448) requires DC +24 V to operate properly. For the work described in this thesis, this voltage was provided by a variable output DC power supply (Hewlett Packard 6002A) operating in constant voltage mode. This could be replaced by another power supply capable of outputting the required voltage should it be necessary. In order to maximize the effectiveness of the thermocouple, it is advised that a thermally conductive paste be applied to the inside of the channel containing the

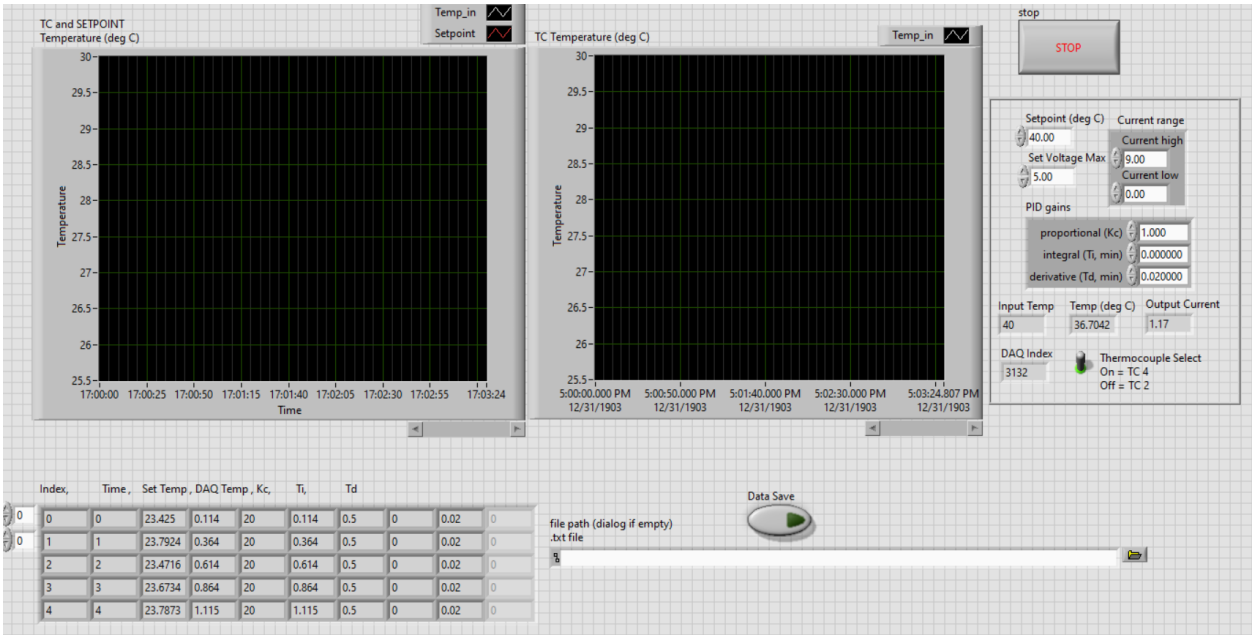

Figure A.1 The front panel of the VI used to operate the heating stage.

thermocouple to ensure good thermal contact is made.

The signal from the transducer is sent on to a computer through a DAC board employing a GPIB connection. From there, the amount of current to be applied to the heating element is determined by a LabVIEW VI. This VI and required subVIs are located on the lab computers, under "C:\Heater Control LabVIEW VIs", and online at https://byu.box.com/s/ii07ncsn286vwke9r9yefzcka5djdm53. The main VI is "Microfluidic_temperature_currentPID_physics.vi". Required subVIs and control files are stored alongside the main VI. They are as follows: "Control.ctl", "Number to HexSDP Address.vi", "Set Current.vi", "Set Output.vi", and "Set Voltage.vi".

An image of the main VI front panel is shown in Fig. A.1. The current temperature and the setpoint temperature are shown in the two graphs. Temperature data can be saved using the button and address bar at the bottom right. Operation is done using the box at the right hand side of the panel. All values that can be set by the user appear in boxes with white backgrounds. The numbers currently shown are the default values. These will reset back to the defaults every time the program

is opened. It is advised to keep a separate record of effective parameters so they are not lost upon re-opening of the VI. The maximum voltage and current range parameters are dependent on the power supply being controlled. For the one used in this thesis (BK Precision 1696) the maximum output is 20 V and 10 A. Those values should not be exceeded.

PID values will need to be recalibrated for each new sample as the heating and cooling rates will vary. That said, it is advised to keep the values small, less than or equal to 1, to allow the controller to make full use of the range available to it. Too high of values result in the output current jumping between the two extremes of the allowed range, limiting the effectiveness of the controller. Once good PID values have been determined, the controller can be made to settle faster by narrowing the allowed current range. For any given temperature, there exists a current that if used constantly will result in the system settling on the desired temperature. While that current may not be easily determined, use of a smaller current range roughly centered on that current greatly speeds up the control process. A range spanning roughly 2 amps was found to be effective.

The necessary output current is supplied by a DC power source (BK Precision 1696) controlled by the same VI. This power supply is connected to the computer by a nine-pin serial connection. This connection must be made through a serial port on the computer. A serial to USB adapter will not function properly. The galinstan heating element is accessed via two wires connected to the chip via soldered connections. Before operation, check the quality of these connections. They can be fragile and may need to be reconnected. A poor connection will cause power to be lost outside the sample, reducing the effectiveness of the heating.

Bibliography

[1] T. Baldacchini, *Three-Dimensional Microfabrication Using Two-Photon Polymerization: Fundamentals, Technology, and Applications*, *Micro and Nano Technologies* (Elsevier Science, 2015).

[2] M. Quintanilla and L. M. Liz-Marzán, "Guiding Rules for Selecting a Nanothermometer," Nano Today **19,** 126 – 145 (2018).

[3] P. K. Chow, R. B. Jacobs-Gedrim, J. Gao, T.-M. Lu, B. Yu, H. Terrones, and N. Koratkar, "Defect-Induced Photoluminescence in Monolayer Semiconducting Transition Metal Dichalcogenides," ACS Nano **9,** 1520–1527 (2015), pMID: 25603228.

[4] X.-d. Wang, O. S. Wolfbeis, and R. J. Meier, "Luminescent probes and sensors for temperature," Chem. Soc. Rev. **42,** 7834–7869 (2013).

[5] Picoquant, *TimeHarp 260 User's Manual and Technical Data.*

[6] W. Becker, A. Bergmann, M. Hink, K. König, K. Benndorf, and C. Biskup, "Fluorescence lifetime imaging by time-correlated single-photon counting," Microscopy Research and Technique **63,** 58–66 (2004).

[7] D. Phillips, R. Drake, D. O'Connor, and R. Christensen, "Time Correlated Single-Photon Counting (TCSPC) Using Laser Excitation," Instrumentation Science & Technology **14,** 267–292 (1985).

[8] K. B. Lee, J. Siegel, S. Webb, S. Lévêque-Fort, M. Cole, R. Jones, K. Dowling, M. Lever, and P. French, "Application of the Stretched Exponential Function to Fluorescence Lifetime Imaging," Biophysical Journal **81,** 1265 – 1274 (2001).

[9] C. Lewis, "Neural Network Approximations of the Temperature of CdTe Quantum Dots," Senior Thesis, Brigham Young University (2020).

Index